Journal of the Korean Physical Society, Vol. 47, No. 6, December 2005, pp. 997∼1001

Guided Dispersions and Single-Mode Operations of Surface Plasmon Polaritons through Subwavelength Plasmonic Holes

Ki Young Kim,* Young Ki Cho and Heung-Sik Tae
School of Electrical Engineering and Computer Science, Kyungpook National University, Daegu 702-701

Jeong-Hae Lee
Department of Radio Science and Communication Engineering, Hongik University, Seoul 121-791

(Received 26 July 2005)

The guided dispersion characteristics of surface plasmon polaritons (SPPs) through subwavelength plasmonic holes (SPHs) in metals are investigated with an emphasis on their single- mode operations. Using a characteristic equation without any modifications, we obtained the dispersion curves of SPPs for several diametric SPHs, thereby providing a variety of information, such as the dispersions, the allowed spectral ranges, the cutoff frequencies, the wave velocities, and so on. The significant effect of SPH diameter on single-mode operations is analyzed.

PACS numbers: 71.36.+c, 42.25.Bs, 84.40.Az
Keywords: Dispersion, Surface plasmon polariton, Subwavelength hole

I. INTRODUCTION

The recent attention that has been paid to enhanced light transmission through a subwavelength single hole [1–7] and subwavelength hole arrays [8–12] in thick metal films of finite thickness is due to both a fundamental interest in extraordinary phenomena that contradict standard aperture theory [13–15] and the broad spectrum of potential applications, such as wavelength-tunable filters, optical modulators, spatial and spectral multiplexing, coupling in and out of optical fibers, near-field optical microscopes, subwavelength photolithography, flat-panel displays, and ultrahigh-density optical data storage, resulting from the pioneering experimental work of T. W. Ebbesen *et al.* in 1998 [8]. Theoretical analyses [4,7,9,10,12,16,17] and experimental evidence [1–3,5,6,8, 11] have already been presented to elucidate the anomalous phenomena, wherein the throughput process in thick metal films from one side to the other involves the excitation of surface plasmon polaritons (SPPs) from plane wave illuminations at the entrance aperture, the propagation of the SPPs through hollow metallic channels with a finite length, and the de-excitation of the SPPs at the exit aperture. As such, the extraordinarily high transmission of light through the hollow metallic channels can either be associated with an efficient energy conversion between the SPPs and the free space modes of the incident or transmitted regions [18] or with certain resonance phenomena [11,12,16,17] related to hollow metallic channels with finite dimensions.

Nonetheless, the guidance of the SPPs through the hollow metallic channels plays a crucial role in the entire "extraordinary throughput" system. In addition, the transmission of SPPs through hollow channels is also of great importance for novel types of light manipulating devices with subwavelength scales [19–22], negative dielectric cladding [20, 21, 23, 24], or even metamaterial cladding [22,25], which have various applications, including compact signal transmission lines and sharp bends for nanophotonics. Consequently, an analysis of the fundamental guided dispersion characteristics of SPPs through hollow channels is indispensable to both the guiding structure itself and its associated structures, *e.g.*, previous enhanced throughput systems.

Accordingly, this paper numerically investigates the guided dispersion characteristics and the associated frequency region for the single-mode operation of SPPs through the free space of circular holes with different diameters surrounded by metal. Bulk gold was selected as the surrounding metal, because the frequency-dependent nature of its dielectric constant at optical frequencies can be assumed using the Drude model. Therefore, based on the well-developed characteristic equation without any approximations, several rigorous dispersion curves are obtained for SPPs for each azimuthal eigenvalue; then, their propagation characteristics are discussed.

*E-mail: doors@ee.knu.ac.kr

II. SUBWAVELENTH PLASMONIC HOLE (SPH) USING BULK GOLD

Figure 1 shows a schematic illustration of a circular hole with a diameter of $D = 2a$, where the hollow core ($r < a$, region 1) and the infinite cladding ($r > a$, region 2) are the free space and the metal, respectively. The diameter of the hole was smaller than the operating wavelength (subwavelength, *i.e.*, $D < \lambda$), which will be shown in the next section. The relative permeability of both regions and the relative permittivity of the free-space region were unity; *i.e.*, $\mu_{r1} = \mu_{r2} = \varepsilon_{r1} = 1.0$. The Drude model was employed to describe the relative permittivity of the metal; *i.e.*, $\varepsilon_{r2} = 1 - \omega_p^2/[\omega(\omega - j\omega_c)]$, where ω_p is the plasma frequency and ω_c is the collision frequency. Due to the plasma-like frequency response of the metal at optical frequencies, together with the subwavelength diametric dimensions, the structure in Figure 1 is called a subwavelength plasmonic hole (SPH). Here, bulk gold was employed to investigate the propagation characteristics of SPPs through SPHs. The plasma

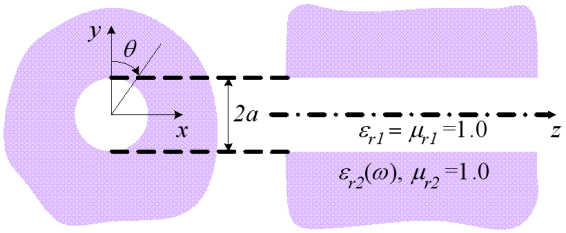

Fig. 1. Schematic illustration of a subwavelength plasmonic hole (SPH). The hollow core and the infinite cladding are the free space and the metal, respectively. The frequency response of the metal's relative permittivity is described using the Drude model.

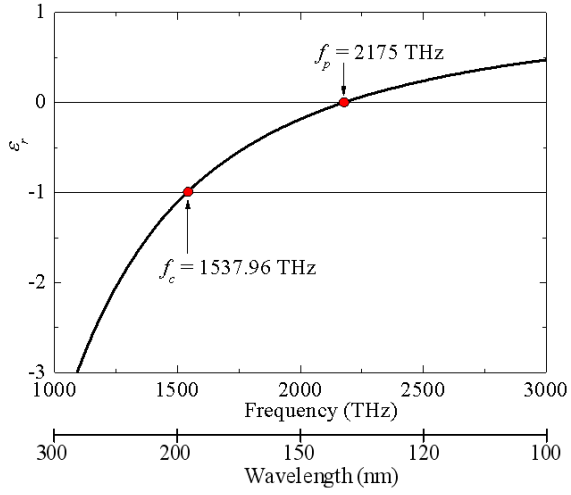

Fig. 2. Relative permittivity of bulk gold. Below the plasma frequency, the relative permittivity is negative. There is a critical frequency of 1537.96 THz, where the relative permittivity is negative unity.

frequency of bulk gold was available in Ref. 26, *i.e.*, $f_p = \omega_p/2\pi = 2175$ THz. (In Ref. 26, the collision frequency of bulk gold is also given as $f_c = \omega_c/2\pi = 6.5$ THz; however, this value is negligible compared with the plasma frequency and is disregarded here, because it hardly has any affect on the guided dispersion characteristics.) The frequency dispersive nature of the relative permittivity of bulk gold is shown in Figure 2. Below the plasma frequency, *i.e.*, $f < f_p$, the relative permittivity was negative. Also, there was a critical frequency, $f_c = f_p/\sqrt{2} = 1537.96$ THz, where the relative permittivity was negative unity. The role of this critical frequency will be mentioned later in Section III.

Following the ordinary steps to derive the characteristic transcendental equation, *i.e.*, enforcing the continuation of the fields between the free space and the metal, we obtain a characteristic equation of the general form [18].

$$\begin{aligned}&[\frac{\varepsilon_{r1}}{k_1}\frac{I_m'(k_1a)}{I_m(k_1a)} - \frac{\varepsilon_{r2}}{k_2}\frac{K_m'(k_2a)}{K_m(k_2a)}]\\ &\times[\frac{\mu_{r1}}{k_1}\frac{I_m'(k_1a)}{I_m(k_1a)} - \frac{\mu_{r2}}{k_2}\frac{K_m'(k_2a)}{K_m(k_2a)}]\\ &= [\frac{m\beta}{k_0a}(\frac{1}{k_1^2} - \frac{1}{k_2^2})]^2 \end{aligned} \quad (1)$$

This is identical to the characteristic equation of a plasma column [27], although the relative permittivities of the core and the claddings are inverted, where $k_i (i = 1, 2)$ is the transverse propagation constant in each region and is given by $k_i = k_0\sqrt{\bar{\beta}^2 - \mu_{ri}\varepsilon_{ri}}$, $\bar{\beta}(= \beta/k_0)$ is the normalized propagation constant in the propagation direction, k_0 is the free space wave number, $I_m(\cdot)$ and $K_m(\cdot)$ are modified Bessel functions of the first and the second kind, respectively. Prime denotes differentiation, and is the azimuthal eigenvalue. The numerical solutions of Eq. (1) are directly obtained by using Newton's method[1], and the results will be presented in the next section.

III. NUMERICAL RESULTS AND DISCUSSION

Figure 3 shows the dispersion curves for the SPPs through several diametric SPHs, *i.e.*, $D = 150$, 100, 90, 50, and 10 nm, numerically obtained using the characteristic equation, Eq. (1). The first three eigenmode solutions attained were for TM-like modes, *i.e.*, TM_{01}, HE_{11}, and HE_{21}, and corresponded to $m = 0$, 1, and 2, respectively. No TE-like modes existed for the selected material parameters. In Figure 3, auxiliary wavelength abscissas were added underneath the frequency axes for

[1] MATHEMATICA (ver. 4.0) from Wolfram Research, Inc., was used throughout this paper.

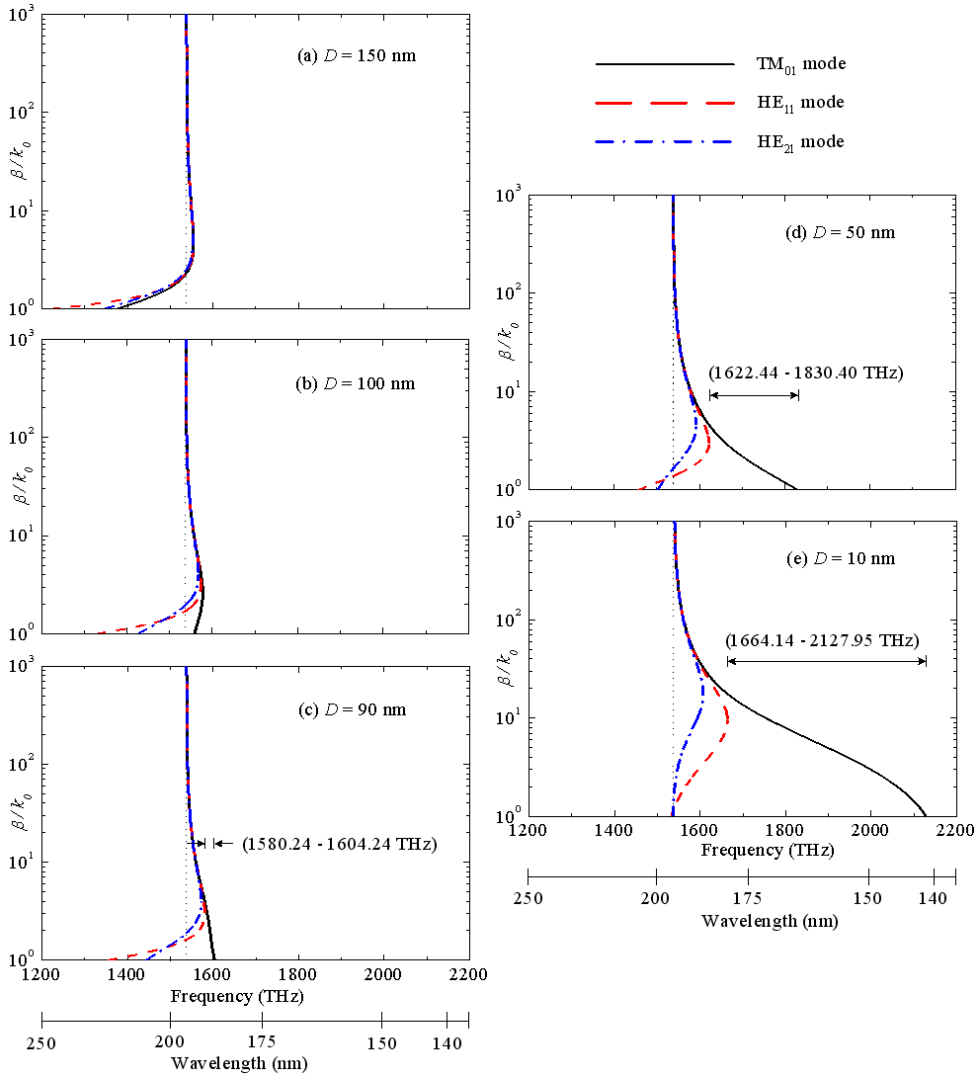

Fig. 3. Dispersion curves of SPPs through SPHs: (a) $D = 150$ nm, (b) $D = 100$ nm, (c) $D = 90$ nm, (d) $D = 50$ nm, and (e) $D = 10$ nm. The vertical dotted lines represent the critical frequency $f_c = 1537.96$ THz, below which no backward wave solutions exist. For a comparison between the operating wavelength and the SPH diameter, auxiliary wavelength abscissas are added underneath the frequency axes.

a comparison between the operating wavelengths and the SPH diameters. It was noted that eigenvalue solutions still existed for the SPPs when using SPHs with much smaller diameters, which is not the case for an ordinary circular waveguide with a perfect electric conductor [28].

As in the case of a plasma column (same structure, except the relative permittivities are inverted), the eigenvalue solutions for the corresponding azimuthal eigenvalues m were monomodal; *i.e.*, only principal modes existed for each azimuthal eigenvalue. (No solutions existed for higher-order modes, such as TM_{0n} and HE_{mn} $(n > 1)$.) The positive and the negative slopes of the dispersion curves corresponded to forward and backward traveling waves, respectively [22]. No backward waves existed below the critical frequency, *i.e.*, $f_c = 1537.96$ THz, as shown by vertical dotted lines in Figure 3, where the relative permittivity was negative unity, as shown in Figure 2. Low-frequency cutoffs for the backward waves occurred at this critical frequency while this frequency is the high-frequency cutoff point in the case of a plasma column; *i.e.*, no solutions exist when $f > f_c$ [29]. As the frequency approached the critical frequency, the normalized propagation constant of backward waves asymptotically approached a vertical line at $f_c = 1537.96$ THz, which corresponded to extremely slow phase velocities because the normalized propagation constant is the reciprocal of the normalized phase velocity; *i.e.*, $v_p/c = k_0/\beta$, where c is the speed of light. In contrast to the case of backward waves, forward waves were observed to exist both below and above the critical frequency.

The cutoff frequencies for the TM_{01}, HE_{11}, and HE_{21} modes, at which $\beta/k_0 = 1.0$, are listed in Table 1.

Table 1. Cutoff frequencies of SPPs through SPHs. The unit is THz.

Diameter of SPH	TM_{01}	HE_{11}	HE_{21}
$D = 150$ nm	1375.24	1222.25	1345.17
$D = 100$ nm	1558.58	1332.09	1426.63
$D = 90$ nm	1604.24	1356.33	1442.85
$D = 50$ nm	1830.40	1456.61	1501.99
$D = 10$ nm	2127.95	1533.21	1536.31

As the diameter of the SPH was decreased, these cutoff frequencies shifted toward higher frequencies and $f_{cut}^{TM_{01}} > f_{cut}^{HE_{21}} > f_{cut}^{HE_{11}}$, resulting in a crossing point for the dispersion curves between the HE_{11} and the HE_{21} modes, as shown in Figure 3.

For hybrid modes ($m \geq 1$), forward and backward waves always coexisted and met at certain bifurcation frequencies, above which no solutions were allowed. Thus, the bifurcation frequency of the HE_{11} mode, in particular, played the role of a lower limit for single-TM_{01}-mode operation, which will be mentioned later. In contrast, only backward waves existed for the symmetrical modes ($m = 0$) when the diameters of the SPHs were sufficiently small. For certain larger SPHs, such as $D = 150$ nm and $D = 100$ nm, as shown in Figures 3(a) and (b), respectively, forward, as well as backward, waves were observed in the TM_{01} mode, as in the case of the hybrid modes. In the case of a plasma column, the coexistence of forward and backward waves can only be observed in hybrid modes under certain limited circumstances [28]. The existence of a forward TM_{01} mode with $D = 150$ nm and $D = 100$ nm resulted in a very negligible spectral range for single-TM_{01}-mode operations. Meanwhile, in the case of $D = 90$ nm in Figure 3(c), the forward TM_{01} mode disappeared, and only backward waves with negative slopes existed. Therefore, the frequency region for single-TM_{01}-mode operation was considered as the spectral region range from the bifurcation frequency between the forward- and the backward-wave regions of the HE_{11} mode to the cutoff frequency of the TM_{01} modes, *i.e.*, 1580.24 to 1604.24 THz, as shown in Figure 3(c).

In the case of conventional circular dielectric waveguides [30] or recent subwavelength-diameter wire waveguides [31], the fundamental mode of single-mode-operation is the HE_{11} mode, which has no lower cutoff frequency. However, a single-mode operation could be achieved with the present structure by using the TM_{01} mode due to the material dispersion of the cladding.

For the smaller SPHs, *i.e.*, when $D = 50$ nm in Figure 3(d), the backward wave region of the TM_{01} mode was stretched to higher frequencies (1830.40 THz). Thereby, the frequency region for the backward-TM_{01}-single-mode operation became broader than when $D = 90$ nm, *i.e.*, 1622.44 to 1830.40 THz. In the case of much smaller diameters, (*i.e.*, $D = 10$ nm), as shown in Figure 3(e), the frequency region for the single-TM_{01}-mode operation was much broader and ranged from 1664.14 to 2127.95 THz. As the SPH diameter was decreased, the cutoff frequency for the TM_{01} mode (higher limit of the single-TM_{01}-mode operation region) shifted toward higher frequencies much more than the bifurcation frequency of the HE_{11} mode (lower limit of the single-TM_{01}-mode operation region) did. As a result, the frequency region for the single-TM_{01}-mode operation became broader as the SPH diameter was decreased. From Maxwell's equation, the axial electric fields of the TM_{01} mode along the core and the cladding regions can be expressed with modified Bessel functions of the first and the second kinds, respectively, as $E_{z1} = AI_0(k_1 r)\exp[j(\omega t - \beta z)]$ and $E_{z2} = BK_0(k_2 r)\exp[j(\omega t - \beta z)]$. A and B are constants. If we consider the field distributions with respect to the radial direction (r), the fields increase with exponential-like behaviors ($I_0(\cdot)$ and $K_0(\cdot)$) as the field position is nearer the interface. In other words, the fields at the interface between the core and the cladding, *i.e.*, at $r = a$, take on their maximum values, which is a typical property of SPPs. Furthermore, the fields are more confined at the interface as the normalized propagation constants have higher values due to the expression of the transverse propagation constants, *i.e.*, $k_i = k_0\sqrt{\bar{\beta}^2 - \mu_{ri}\varepsilon_{ri}}$. In other words, higher normalized propagation constants generate higher transverse propagation constants, which again make the field confinement at the interface even tighter. Other field components of the TM_{01} mode, *i.e.*, E_{ri} (radial electric field) and $H_{\theta i}$ (azimuthal magnetic field), are also governed by the same functions (modified Bessel functions of the first and the second kinds). Thus, the higher normalized propagation constants directly lead to tighter field confinements near the interface between the core and the cladding. If Figures 3(d) and (e) are compared, the normalized propagation constants of the TM_{01} mode for the case $D = 10$ nm of can be seen to be higher than those for the case of $D = 50$ nm at the same operating frequency, *e.g.*, $f = 1700$ THz at or $f = 1800$ THz, which directly means that the field confinements at the interface for the $D = 10$ nm case are tighter than those for the $D = 50$ nm case. Thus, at a sufficiently small diameter, a broad spectral range with tight field confinement near the interface was observed for single-TM_{01}-mode operation, which can be used in various waveguide applications.

IV. CONCLUSIONS

The guided dispersion characteristics and associated single-mode operations of SPPs through SPHs with several different diameters were numerically investigated, and a brief comparison was made of SPPs in a plasmonic hole and column. It was interesting to note that there was a critical frequency below which backward waves could not exist. Forward and backward waves always coexisted for hybrid modes. For some larger SPHs, the

forward TM_{01} mode existed, as well as the backward TM_{01} mode, where the forward TM_{01} mode was seen to cause a significant reduction in the frequency range for single-TM_{01}-mode operations. In contrast, as the diameter of the SPH was decreased, the forward TM_{01} mode through the SPHs disappeared at a certain critical diameter while the dispersion curves of the TM_{01} mode were stretched to higher frequencies. As a result, a broader frequency region was provided for single-TM_{01}-mode operations, along with a tight confinement of the guided power at the hole interface, which is expected to be very useful in certain waveguiding applications, *e.g.*, sharp bends in nanophotonic areas [32,33]. Although this paper employed the Drude model of bulk gold to investigate the dispersion characteristics of SPPs through SPHs, the general properties observed here can also be applied to other SPHs made of various plasmonic materials.

ACKNOWLEDGMENTS

This work was supported by grant No. R01-2004-000-10158-0 from the Basic Research Program of the Korea Science & Engineering Foundation.

REFERENCES

[1] D. E. Grupp, H. J. Lezec, T. Thio and T. W. Ebbesen, Adv. Mater. **11**, 860 (1999).
[2] T. Thio, K. M. Pellerin, R. A. Linke, H. J. Lezec and T. W. Ebbesen, Opt. Lett. **26**, 1972 (2001).
[3] H. J. Lezec, A. Degiron, E. Devaux, R. A. Linke, L. Martin-Moreno, F. J. Garcia-Vidal and T. W. Ebbesen, Science **297**, 820 (2002).
[4] F. J. Garcia de Abajo, Opt. Express **10**, 1475 (2002).
[5] A. Degiron, H. J. Lezec, N. Yamamoto and T. W. Ebbesen, Opt. Commun. **239**, 61 (2004).
[6] A. Agrawal, H. Cao and A. Nahata, Opt. Express **13**, 3535 (2005).
[7] N. Bonod, E. Popov and M. Neviere, Opt. Commun. **245**, 355 (2005).
[8] T. W. Ebbesen, H. J. Lezec, H. F. Ghaemi, T. Thio and P. A. Wolff, Nature **391**, 667 (1998).
[9] L. Martin-Moreno, F. J. Garcia-Vidal, H. J. Lezec, K. M. Pellerin, T. Thio, J. B. Pendry and T. W. Ebbesen, Phys. Rev. Lett. **86**, 1114 (2001).
[10] L. Martin-Moreno and F. J. Garcia-Vidal, Opt. Express **12**, 3619 (2004).
[11] H. Cao and A. Nahata, Opt. Express **12**, 1004 (2004).
[12] S. Astilean, P. Lalanne and M. Palamaru, Opt. Commun. **175**, 265 (2000).
[13] H. A. Bethe, Phys. Rev. **66**, 163 (1944).
[14] C. J. Bouwkamp, Philips Res. Rep. **5**, 321 (1950).
[15] C. J. Bouwkamp, Rep. Prog. Phys. **17**, 35 (1954).
[16] W. C. Tan, T. W. Preist and J. R. Sambles, Phys. Rev. B **62**, 11134 (2000).
[17] Y. Takakura, Phys. Rev. Lett. **86**, 5601 (2001).
[18] A. V. Klyuchnik, S. Y. Kurganov and Y. E. Lozovik, Phys. Solid State **45**, 1327 (2003).
[19] D. F. Pile and D. K. Gramotnev, Opt. Lett. **30**, 1186 (2005).
[20] D. K. Qing and G. Chen, Phys. Rev. B **71**, 153107 (2005).
[21] R. Zia, M. D. Selker, P. B. Catrysse and M. L. Brongersma, J. Opt. Soc. Am. A **21**, 2442 (2004).
[22] K. Y. Kim, J. H. Lee, Y. K. Cho and H. S. Tae, Opt. Express **13**, 3653 (2005).
[23] B. Prade and J. Y. Vinet, J. Lightwave Technology **12**, 6 (1994).
[24] B. Prade, J. Y. Vinet and A. Mysyrowicz, Phys. Rev. B **44**, 13556 (1991).
[25] G. D'Aguanno, N. Mattiucci, M. Scalora and M. J. Bloemer, Phys. Rev. E **71**, 046603 (2005).
[26] S. Linden, C. Enkrich, M. Wegener, J. Zhou, T. Koschny and C. M. Soukoulis, Science **306**, 1351 (2004).
[27] W. P. Allis, S. J. Buchsbaum and A. Bers, *Waves in Anisotropic Plasmas* (The MIT Press, Cambridge, 1963), p. 215.
[28] D. M. Pozar, *Microwave Engineering*, 2nd ed. (Wiley, New York, 1998), Chap. 3.
[29] V. L. Granatstein, S. P. Schlesinger and A. Vigants, IEEE Trans. Antennas Propag. **11**, 489 (1963).
[30] D. Marcuse, *Light Transmission Optics*, 2nd ed. (Van Nostrand-Reinhold, New York, 1982), p. 303.
[31] L. Tong, J. Lou and E. Mazur, Opt. Express **12**, 1025 (2004).
[32] S. H. Han, Q. H. Park, Y. S. Park, Y. Roh and H. S. Jeon, J. Korean Phys. Soc. **45**, 9 (2004).
[33] S. H. Han, Q. H. Park, Y. S. Park, Y. Roh and H. S. Jeon, J. Korean Phys. Soc. **45**, 112 (2004).